SLAC – PUB – 3660
April 1985
(A)

SUPERCONVERGENT TRACKING AND INVARIANT SURFACES IN PHASE SPACE*

R. D. RUTH, T. RAUBENHEIMER
Stanford Linear Accelerator Center, Stanford University, Stanford, CA, 94305
R. L. WARNOCK
Lawrence Berkeley Laboratory, University of California, Berkeley, CA, 94720

INTRODUCTION

The question of long term beam stability in very large storage rings presents an extraordinary challenge in nonlinear dynamics. Since current computational methods seem less than adequate on the long time scales involved, we have undertaken a program of evaluating several methods that either are new or have not been tried in accelerator problems heretofore.

The methods we investigate fall into two categories: (1) iteration of maps describing concatenated machine elements , for tracking of single particles, and (2) infinite-time methods for direct computation of invariant surfaces in phase space. Our various proposals can be described briefly as follows:

1. Tracking, finite time
   (a) 'superconvergent tracking', an adaptation of Kolmogorov-Arnol'd-Moser (KAM) perturbation theory to the finite time problem.
   (b) Local integration of the Hamilton-Jacobi (HJ) equation with respect to the time, the equation being viewed as a system of ordinary differential equations for angle-variable Fourier modes of the generating function.
2. Invariant surfaces, infinite time
   (a) The original KAM superconvergent perturbation theory.
   (b) Iterative solution of the HJ equation stated as a system of algebraic equations for the Fourier modes of the generating function.
   (c) Solution of the equation of (2b) by Newton's method.

Items (1a) and (2b) may be realized in two ways, either in a conventional quasi-analytic fashion or by a new numerical technique in which complexity does not increase as the calculation is carried to higher orders. The present report is concerned with item (1a) in the quasi-analytic realization, and with item (2b).

INVARIANT SURFACES THROUGH ITERATIVE SOLUTION OF THE HAMILTON-JACOBI EQUATION

In action-angle variables $(\mathbf{J},\boldsymbol{\phi})$ the Hamiltonian of a perturbed integrable system is written as

$$H(\boldsymbol{\phi},\mathbf{J},\theta) = H_0(\mathbf{J}) + F(\boldsymbol{\phi},\mathbf{J},\theta) \ , \tag{1}$$

where the perturbation F is periodic with period 2π in $\boldsymbol{\phi}$ and θ , the latter being the machine azimuth. We seek a canonical transformation $(\mathbf{J},\boldsymbol{\phi}) \rightarrow (\mathbf{K},\boldsymbol{\psi})$ in the form

$$\mathbf{J} = \mathbf{K} + G_{\boldsymbol{\phi}}(\boldsymbol{\phi},\mathbf{K},\theta) \ , \tag{2}$$

$$\boldsymbol{\psi} = \boldsymbol{\phi} + G_{\mathbf{K}}(\boldsymbol{\phi},\mathbf{K},\theta) \ , \tag{3}$$

such that the Hamiltonian becomes a function of $\mathbf{K}$ alone. Bold face characters denote d-dimensional vectors and subscripts indicate partial differentiation. The new action $\mathbf{K}$ will be invariant, and the new angle $\boldsymbol{\psi}$ will advance linearly with θ. The HJ equation to determine G is the requirement that the new Hamiltonian H indeed depend only on $\mathbf{K}$; namely,

$$H_0(\mathbf{K}+G_{\boldsymbol{\phi}}) + F(\boldsymbol{\phi},\mathbf{K}+G_{\boldsymbol{\phi}},\theta) + G_\theta = H_1(\mathbf{K}) \ . \tag{4}$$

Once G is known, the invariant surfaces $\mathbf{J} = \mathbf{J}(\boldsymbol{\phi},\theta)$ may be plotted directly from (2), with the constant $\mathbf{K}$ as an input parameter.

We look for periodic solutions of Eq. (4) in the form

$$G(\boldsymbol{\phi},\mathbf{K},\theta) = \sum_{\mathbf{m},n=-\infty}^{+\infty} g_{\mathbf{m}n}(\mathbf{K}) e^{i(\mathbf{m}\cdot\boldsymbol{\phi}-n\theta)} \ . \tag{5}$$

Let us rewrite Eq. (4), by adding and subtracting the first two terms in the Taylor series of $H_0(\mathbf{K}+G_{\boldsymbol{\phi}})$:

$$\begin{aligned} &\boldsymbol{\nu}\cdot G_{\boldsymbol{\phi}} + G_\theta = \\ &\quad -[H_0(\mathbf{K}+G_{\boldsymbol{\phi}}) - H_0(\mathbf{K}) - \boldsymbol{\nu}\cdot G_{\boldsymbol{\phi}} + F(\boldsymbol{\phi},\mathbf{K}+G_{\boldsymbol{\phi}},\theta)] \\ &\quad +[H_1(\mathbf{K}) - H_0(\mathbf{K})] \ , \end{aligned} \tag{6}$$

where $\boldsymbol{\nu}$ is the zeroth-order tune,

$$\boldsymbol{\nu}(\mathbf{K}) = \frac{\partial H_0(\mathbf{K})}{\partial \mathbf{K}} \ . \tag{7}$$

If we now take the Fourier transform of Eq. (6), the result for $\mathbf{m} \neq 0$ is

$$\begin{aligned} g_{\mathbf{m}n} = \frac{i}{(\mathbf{m}\cdot\boldsymbol{\nu}-n)} \frac{1}{(2\pi)^{d+1}} \int_0^{2\pi} d\boldsymbol{\phi}\, d\theta\, e^{-i(\mathbf{m}\cdot\boldsymbol{\phi}-n\theta)} \times \\ \left[H_0(\mathbf{K}+G_{\boldsymbol{\phi}}) - H_0(\mathbf{K}) - \boldsymbol{\nu}\cdot G_{\boldsymbol{\phi}} + F(\boldsymbol{\phi},\mathbf{K}+G_{\boldsymbol{\phi}},\theta)\right] \ . \end{aligned} \tag{8}$$

Since $\mathbf{m} \neq 0$ in Eq. (8), the $\boldsymbol{\phi}$ - independent term $H_1 - H_0$ of Eq. (6) does not contribute. Furthermore, since $G_{\boldsymbol{\phi}}$ does not have an $\mathbf{m} = 0$ component, Eq. (8) constitutes a closed set of equations for the $g_{\mathbf{m}n}$ for $\mathbf{m} \neq 0$. We solve this system by simple iteration, taking $G_{\boldsymbol{\phi}} = 0$ on the right-hand side at the first step.

Once $G_{\boldsymbol{\phi}}$ is known, H_1 can be obtained by averaging the left-hand side of Eq. (4) over $\boldsymbol{\phi}$ and θ since G_θ averages to zero. The fully perturbed tune is then

$$\boldsymbol{\nu}_1(\mathbf{K}) = \frac{\partial H_1(\mathbf{K})}{\partial \mathbf{K}} \ , \tag{9}$$

which gives the evolution of the new angle variable,

$$\boldsymbol{\psi} = \boldsymbol{\psi}_0 + \boldsymbol{\nu}_1\theta \ . \tag{10}$$

Finally, g_{0n} for $n \neq 0$ is determined by the Fourier transform of Eq. (4) for $\mathbf{m} = 0$. The single coefficient g_{00} remains as a free parameter and can be set to zero without loss of generality. The detailed time evolution of the system, usually of less interest than invariant surfaces, can be obtained by solving Eq. (3) for $\boldsymbol{\phi}$ as a function of $\boldsymbol{\psi}$ and θ and then substituting into Eq. (2).

For numerical calculations we truncate the Fourier series in Eq. (5) and discretize the integrals over $\boldsymbol{\phi}$ and θ. All sums are then performed as Fast Fourier Transforms. Since $\mathbf{m}\cdot\boldsymbol{\nu} - n$ is a potential small divisor in Eq. (8), $\boldsymbol{\nu}$ must be chosen so that the divisor is not too small in comparison to the corresponding numerator, if convergence is to be achieved.

Currently we have two computer programs that perform the iteration, one for a single degree of freedom and the other for two degrees of freedom; each accepts a general Hamiltonian. We have tested the programs on the isolated resonance model, an integrable example in which a complete set of invariants

* Work supported by the Department of Energy, contracts DE-AC03-76SF00515 and DE-AC03-76SF00098.

Presented at the 1985 Particle Accelerator Conference,
Vancouver, B.C., Canada, May 13-16, 1985

(not identical to K above) can be written down explicitly. Checking that the invariants are indeed constant (to a level of accuracy consonant with the accuracy in solving Eq. (8)) is a nontrivial test of the computation, which is passed successfully.

In Fig. 1a we show results in one degree of freedom for the isolated resonance model,

$$H = \nu_0 J + \alpha J^2/2 + \epsilon J^{m/2}\cos(m\phi - n\theta) \qquad (11)$$

for $m = 4$ and $n = 1$. $J^{1/2}\sin\phi$ is plotted against $J^{1/2}\cos\phi$ for two different values of K, where J is obtained as a function of ϕ (at fixed $\theta = 0$) from Eq. (2). The parameters were chosen to illustrate that the method can handle large orbit distortions very close to a resonance. The two curves, which hug the separatrix on either side of the resonance island, have $\nu = \nu_0 + \alpha K = .24812, .2519$. At such close proximity to a resonance, the value of ϵ chosen is close to the maximum that will allow convergence of the iteration; farther from resonance much bigger values of ϵ can be tolerated (for instance values such that the maximum of F is about 20% of H_0). In the example of Fig. 1a, 12 iterations sufficed to solve Eq. (8) to an accuracy $\delta = .001$ where at the p^{th} iteration

$$\delta \equiv \frac{\|g^{(p+1)} - g^{(p)}\|}{\|g^{(p)}\|} , \qquad (12)$$

the norm $\|\ \|$ being the sum of absolute values of the components of $g = [g_{mn}]$. The mode truncation for this case was $|m| \leq 32$, $|n| \leq 32$; however, with only 8 modes each for m and n the graphs appear the same to the eye. The analytic invariant was constant to about 3 digits. Farther from resonance, say one full resonance width away, one obtains a much smaller δ with fewer iterations.

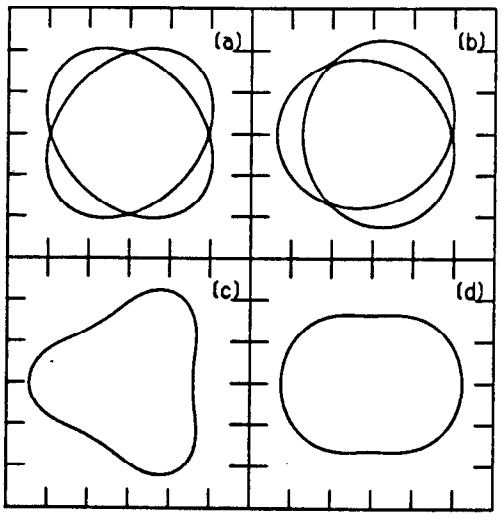

Fig. 1 (a) Invariant curves at $\theta = 0$ for Eq. (11) with $m = 4$, $n = 0$, $\nu_0 = 0.24$, $\alpha = 0.01$, $\epsilon = 2.25 \times 10^{-4}$. (b) Invariant curves at $\theta = 0$ for Eq. (13) with $\nu_0 = 1.28333$, $\alpha = 0.05$, $\epsilon = 7.4 \times 10^{-2}$. (c), (d) Surfaces of section for Eq. (14) with $\nu_1 = 0.68411$, $\nu_2 = 0.49313$, $\epsilon = 0.01$, $K_1 = K_2 = 1.0$.

Fig. 1b is a non-integrable case with an x^3 perturbation,

$$H = \nu_0 J + \alpha J^2/2 + \epsilon J^{3/2}\cos^3\phi\ \sin^4\theta , \qquad (13)$$

evaluated near a third order resonance $n/m = 4/3$. There are fairly strong modes $(m,n) = (1,0)$, $(1,2)$ in addition to the dominant mode $(3,4)$. The figure shows the typical behavior of a third order resonance with strong nonlinear detuning. Note that the curves shown once again follow the separatrix.

In Figs. 1c and 1d we plot results in two degrees of freedom for the 'difference coupling resonance' model,

$$H = \nu_1 J_1 + \nu_2 J_2 + \epsilon J_1^{3/2} J_2 \cos(3\phi_1 - 2\phi_2 - \theta) , \qquad (14)$$

for a single choice of the pair of invariants K_1 and K_2. The plots are 'surfaces of section' for $\phi_i = \theta = 0$, first for $i = 1$, then for $i = 2$. Such plots promise to be quite informative, providing information that cannot be obtained by tracking if there is more than one degree of freedom; (in tracking, it is difficult to choose initial conditions so as to populate appreciably the section $\phi_i = \theta = 0$). Our experience regarding convergence and mode truncation in Figs. 1b,c, and d is similar to that described above for Fig. 1a.

SUPERCONVERGENT TRACKING

The aim of superconvergent tracking is to calculate a map which takes the initial conditions at one point in a magnetic lattice to final conditions at some other point. For a circular accelerator or storage ring, one would like to calculate the map for a significant fraction of an entire turn. Once this map is obtained, it can be iterated numerically to discover long term behavior. This complements the infinite time approach in that stochastic behavior and instability can be studied.

The map is generated by a sequence of canonical transformations so that the Hamiltonian after n steps is zero through some order in the perturbation strength. If the Hamiltonian is zero, then the new variables are simply constant and can be used as initial conditions. The map is then obtained by applying the transformations in reverse order. This, in effect, solves the Hamiltonian-Jacobi equation for a finite interval in the independent variable.

We begin with the Hamiltonian for linear motion perturbed by a small nonlinear part:

$$H = \nu \cdot \mathbf{J} + F(\phi, \mathbf{J}, \theta) . \qquad (15)$$

It is most convenient to work in the 'interaction representation' which is accomplished with the transformation

$$\begin{aligned} \phi_0 &= \phi - \nu\theta \\ \mathbf{J}_0 &= \mathbf{J} \quad , \end{aligned} \qquad (16)$$

and the new Hamiltonian is given by

$$H = F(\phi_0 + \nu\theta, \mathbf{J}_0, \theta) \equiv F_0(\phi_0, \mathbf{J}_0, \theta) . \qquad (17)$$

F_0 is of course periodic in ϕ, the angle variables, but it is not periodic in θ.

Now we perform the first of a sequence of canonical transformations which are close to the identity,

$$\mathbf{J}_0 = \mathbf{J}_1 + G_{\phi_0}(\phi_0, \mathbf{J}_1, \theta) \qquad (18)$$

$$\phi_1 = \phi_0 + G_{\mathbf{J}_1}(\phi_0, \mathbf{J}_1, \theta) , \qquad (19)$$

which yields the new Hamiltonian

$$H_1 = F_0(\phi_0, \mathbf{J}_1 + G_{\phi_0}, \theta) + G_\theta . \qquad (20)$$

This in turn can be written in the suggestive form

$$\begin{aligned} H_1 =& [F_0(\phi_0, \mathbf{J}_1 + G_{\phi_0}, \theta) - F_0(\phi_0, \mathbf{J}_1, \theta)] \\ &+ [G_\theta + F_0(\phi_0, \mathbf{J}_1, \theta)] \quad . \end{aligned} \qquad (21)$$

Note that the Hamiltonian has temporarily been left in the same mixed variables as G.

Now we would like to find a G so that the Hamiltonian is of higher order in the perturbation strength. If we solve for G such that the second bracket in Eq. (21) is zero, and if F_0 is of order ϵ, then the new Hamiltonian is of order ϵ^2. Completing the substitution, we are left with

$$\begin{aligned} H_1 =& F_0(\phi_0, \mathbf{J}_1 + G_{\phi_0}, \theta) - F_0(\phi_0, \mathbf{J}_1, \theta) \\ \equiv& F_1(\phi_1, \mathbf{J}_1, \theta) \quad . \end{aligned} \qquad (22)$$

At this point we can return to Eq. (17) to repeat the process. Stopping after n steps , we find

$$H_n = F_n(\phi_n, \mathbf{J}_n, \theta) \sim O(\epsilon^{2^n}) \ , \tag{23}$$

and from Hamilton's equations

$$\begin{aligned} \phi_n &= \text{constant} + O(\epsilon^{2^n}) \\ \mathbf{J}_n &= \text{constant} + O(\epsilon^{2^n}) \ . \end{aligned} \tag{24}$$

Thus, provided that ϵ is sufficiently small, ϕ_n and $\mathbf{J}_n$ can be used as initial conditions.

To illustrate the technique let $n = 1$ and consider the first order transformation. The solution for G is

$$G(\phi_0, \mathbf{J}_1, \theta) = -\int_{\theta_i}^{\theta} F_0(\phi_0, \mathbf{J}_1, \theta')d\theta' \ . \tag{25}$$

Note that the limits have been chosen so that $G \to 0$ as $\theta \to \theta_i$. Thus $(\phi_1, \mathbf{J}_1)$ are the initial conditions at $\theta = \theta_i$ with an error of order ϵ^2. Given $(\phi_1, \mathbf{J}_1)$ at θ_i, we can use Eqs. (16), (18) and (19) to calculate $(\phi, \mathbf{J})$ at θ with an error of order ϵ^2. In addition there is another parameter which must not be too large, $\theta - \theta_i \equiv \Delta\theta$. From Eq. (25) there will, in general, be secular terms in G, namely terms that increase linearly with $\Delta\theta$. These must be controlled by keeping $\Delta\theta$ sufficiently small.

This method has been carried out through second order for one dimension and through first order for two dimensions. Our approach is to perform the transformations analytically with the aid of an algebraic manipulation program, REDUCE 3.1, which then directly writes FORTRAN subroutines to evaluate the map numerically. Since the map is an implicit one, it is inverted by Newton's method.

To illustrate we first present the first order method applied to the case of the isolated resonance in Eq. (11). Figures 2a and 2b show one dimensional phase space at $\theta = 0$ for the fourth and sixth order resonance respectively. For the $\Delta\theta$ chosen, the calculated points are essentially identical to the exact solution.

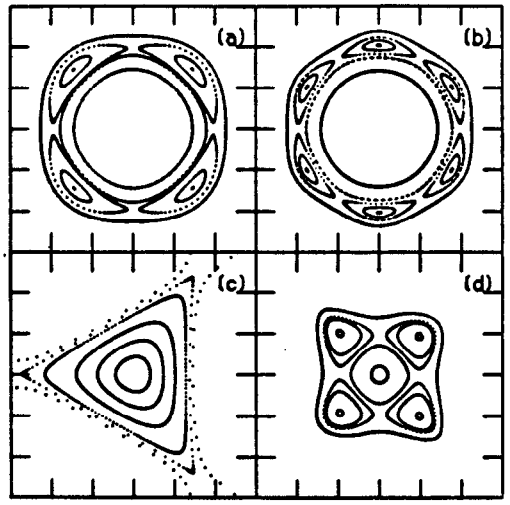

Fig. 2 (a) First Order tracking for Eq. (11) with $(m, n) = (4, 1)$. (b) First order tracking for Eq. (11) with $(m, n) = (6, 1)$. (c) Second order tracking for a sextupole perturbation. (d) Second Order tracking for an octupole perturbation.

To illustrate the second order method we show a sextupole perturbation with a sinusoidally varying strength ($H \sim b_3 x^3 \cos\theta$) in Fig. 2c, and an octupole perturbation with a periodic delta function strength ($H \sim b_4 x^4 \delta_p(s)$) in Fig. 2d. In both cases the tune has been adjusted to be close to the main resonance to enhance the effect of the nonlinearity. Both figures show the expected behavior and agree well with numerical integration.

Finally we show the two dimensional, first order method applied to the case of a sextupole perturbation in the neighborhood of a coupling resonance $2\nu_2 - \nu_1 = k$. Since in this case, the two phase space plots are hard to interpret, we plot the points (ϕ_1, ϕ_2, J_1) in perspective at $\theta = 0$. Fig. 3a shows the plotted points while Fig. 3b shows a ruling of the two-dimensional surface on which the points lie. The existence of the surface (a 2 torus) reflects the presence of two invariants in a near-integrable system, and the fact that all plotted points evolved from one initial state. Figs. 3b and 3c show phase space for the two degrees of freedom separately. We feel that the three-dimensional plot may be quite useful in displaying tracking data.

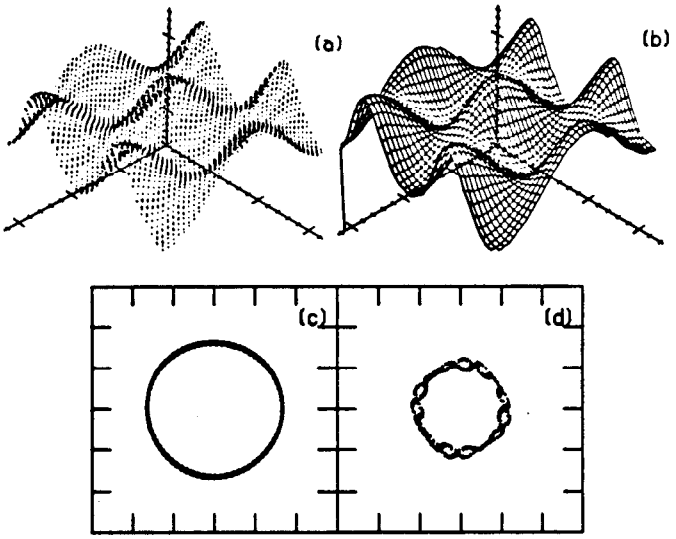

Fig. 3 (a) Points plotted in (ϕ_1, ϕ_2, J_1) space near a coupling resonance. (b) A ruling of the data in (a). (c), (d) Phase space plots of a subset of the data in (a).

We are presently working on a two dimensional, second order program (error $\sim \epsilon^4$) which will use the output of any standard lattice program to calculate the map for some arbitrary fraction of a full turn. In doing so we find integrals of the form

$$I_{lmn}(s) = \int_{s_0}^{s} b_l(s')\beta(s')^{m/2} e^{in(\psi(s') - \psi(s))} ds' \ , \tag{26}$$

as well as higher order integrals such as

$$\int_{s_0}^{s} ds' b_l(s')\beta(s')^{m/2} e^{in(\psi(s') - \psi(s))} I_{pqr}(s') \ . \tag{27}$$

Here $b_l(s)$ is the strength of a $2l$-pole field component, $\beta(s)$ is the beta function, and $\psi(s)$ is the linear betatron phase advance. Because b_l and β are both periodic with period C, the circumference, the integrals are invariant if we shift both s and s_0 by C. Thus, they are calculated once for a lattice and then used to generate the nonlinear map. They also bear a striking resemblance to the integrals which yield nonlinear distortions of invariant curves in standard perturbation theory. This is quite useful in making the connection between the coefficients in a nonlinear map and the distortions of the invariant curves generated by iterating the map.